A Zero-Sequence Component Injection Modulation Method With Compensation for Current Harmonic Mitigation of a Vienna Rectifier

Wenlong Ding, *Student Member, IEEE*, Chenghui Zhang, *Senior Member, IEEE*, Feng Gao, *Member, IEEE*, Bin Duan, *Member, IEEE*, and Han Qiu

***Abstract*—Owing to the operational characteristic of a Vienna rectifier, it is found that the traditional modulation method would result in the current distortion. This paper, therefore, proposes a novel zero-sequence component injection modulation method for improving the input quality of the Vienna rectifier with balanced or unbalanced dc-link voltages. In specific, the degree of unbalanced dc-link voltages increases the size of abnormal regions in a slant and asymmetrical space vector diagram, which leads to more serious current distortion. The proposed method identifies the abnormal intervals by average duties accurately without detecting the position of the reference vector. Considering the operational characteristics, three-phase compensation components are calculated respectively depending on an unbalanced factor and added to three-phase average duties in abnormal intervals. As a result, the current harmonics of the Vienna rectifier are mitigated significantly with balanced or unbalanced dc-link voltages. The effectiveness and the performance of the proposed zero-sequence component injection method for the Vienna rectifier are verified by simulation and experiments.**

***Index Terms*—Current harmonic mitigation, unbalanced dc-link voltages, Vienna rectifier, zero-sequence component injection.**

I. Introduction

With the rapid development of power electronics technology, three-level (3L) rectifiers have been widely used in the applications of the battery chargers, telecommunication power systems, wind turbine systems, and power factor correction systems [1], [2]. Due to the advantages of compact size, simple structure, and control scheme, low voltage stress and high efficiency, a Vienna rectifier is an attractive option for those applications [3]–[5].

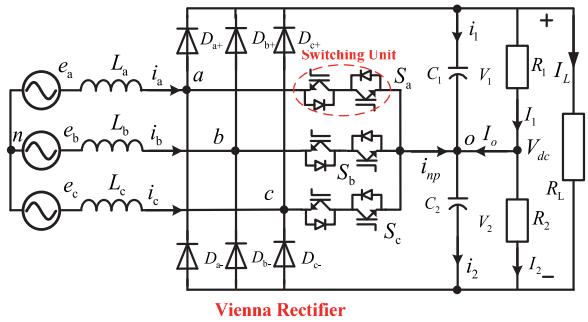

Fig. 1. Typical topology of the Vienna rectifier with dual dc loads.

A typical topology of the Vienna rectifier using bidirectional switches, which is similar to the 3L T-type topology, is shown in Fig. 1, where the dc voltage imbalance may lead to higher stress on semiconductor devices and low-order harmonic pollution in the input currents. Therefore, extensive research works have been carried out focusing on modulation methods [6], [7] to solve these problems. Among these modulation methods, a simple control scheme using the sinusoidal reference current with hysteresis bands was presented in [8] and [9]. However, it is difficult to design the input filters for the drawback of varying switching frequency. On this account, both space vector pulsewidth modulation techniques [10], [11] and carrier-based pulsewidth modulation (CB-PWM) methods [12]–[14] have been widely applied to ensure a constant switching frequency. Another well-understood NP voltage balancing control method presented in [15] and [16] adds the offset voltage with a zero-sequence component to the reference signals. Besides, a hybrid control method combining additional adjustment coefficient is proposed in [17] to suppress the third-order NP voltage fluctuation. Nevertheless, using the above-mentioned processes, which did not consider the operational characteristic of the Vienna rectifier, the input currents are still distorted seriously near the zero-crossing points.

Considering the topological characteristic of the Vienna rectifier, the sign of the input current is the same as that of a control signal owing to the forced commutated current. Based on the previous research works in [12]–[14], *Lee et al.* focused on the operational issues of the Vienna rectifier with the

Manuscript received November 9, 2017; revised January 21, 2018; accepted March 1, 2018. Date of publication March 6, 2018; date of current version November 19, 2018. This work was supported in part by the Major Scientific Instrument Development Program of the National Natural Science Foundation of China under Grant 61527809, in part by the Major International (Regional) Joint Research Project of the National Natural Science Foundation of China under Grant 61320106011, in part by the Joint Funds of the National Natural Science Foundation of China under Grant U1764258 and Grant 61703239, and in part by the Key Research and Development Program of Shandong Province under Grant 2016ZDJS03A02. Recommended for publication by Associate Editor L. Dalessandro. *(Corresponding author: Chenghui Zhang.)*

W. Ding, C. Zhang, B. Duan, and H. Qiu are with the School of Control Science and Engineering, Shandong University, Jinan 250061, China (e-mail: dingwl8804@163.com; zchui@sdu.edu.cn; duanbin@sdu.edu.cn; qiuhan2014@126.com).

F. Gao is with the School of Electrical Engineering, Shandong University, Jinan 250061, China (e-mail: fgao@sdu.edu.cn).

Color versions of one or more of the figures in this paper are available online at http://ieeexplore.ieee.org.

Digital Object Identifier 10.1109/TPEL.2018.2812810

CB-PWM method in detail. A CB-PWM method for Vienna rectifier operation with a variable power factor is proposed in [12] to maintain the sinusoidal input currents. However, the CB-PWM method ignores the possible operational state of the dc voltage imbalance for the Vienna rectifier. Furthermore, compared with a discontinuous pulsewidth modulation (DPWM) method in [11], a simple carrier-based DPWM (CB-DPWM) for the Vienna rectifier was proposed in [13]. This kind of CB-DPWM method guarantees the normal operation of the Vienna rectifier for all modulation index values, while it increases the current harmonic distortion even though the efficiency of the Vienna rectifier increases to a certain extent. As denoted in [14], the CB-PWM method considering structural characteristic needs comprehensive analysis definitely to improve the performance for the Vienna rectifier. The optimized switching vectors, which satisfy operational characteristics of the Vienna rectifier, are selected from the cost function [18] in model predictive control for driving the permanent magnet synchronous generators [19]. However, the unbalanced dc-link voltages may occur in some operating conditions as well, such as switching transients or sudden changes in dual dc loads. More significantly, the dc-link capacitor voltages need to be unbalanced for satisfying the wide range applications in an electric vehicle charging station [20]. Apparently, the low-order current harmonics will be unpredictable as the Vienna rectifier operates under the unbalanced dc-link voltages [21].

In order to solve these problems, the performance of a modulation method to handle unbalanced dc-link voltages should be further discussed to promote the applications of the Vienna rectifier. Recently, 3L inverters aimed at split PV modules with unbalanced dc-link voltage are discussed in photovoltaic systems [22]–[24]. Moreover, independent voltage control, which generates the unbalanced dc-link voltage, is required to expand the application of the rectifier in [25] and [26]. Several studies suppress second- and fourth-order harmonics distinctly when unbalanced dc-link voltages occur [27], [28]. However, not all eight vectors can be utilized to synthetize the reference voltage vector for the Vienna rectifier using the simplified PWM method in [28], which cannot fully suppress the input current distortions for the Vienna rectifier.

Based on the above-mentioned analysis, the compensation method is the most attractive solution for the Vienna rectifier. However, the traditional method only deals with the issue of distortion around a zero-crossing point with balanced dc-link voltages, which is a special case of systems' operation states. The issue of low-order harmonics exists still under the condition of unbalanced dc-link voltages. In addition, two reasons of the current distortion including angle and unbalanced factor are coupled with each other. To propose a general solution and meanwhile address two issues of current distortion around zero-crossing point and low-order harmonics simultaneously, the ranges and components of the compensations should be analyzed in detail and recalculated. Therefore, a zero-sequence component injection modulation method with compensation is proposed in this paper to mitigate the input current distortion caused by the inherent topological characteristics of the Vienna rectifier under both balanced and unbalanced dc-link voltage conditions.

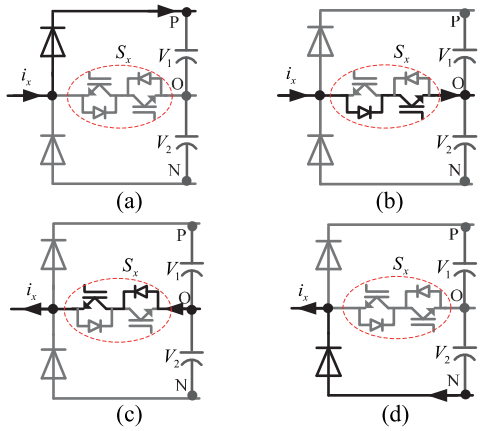

Fig. 2. Current paths depending on the current direction and the switching unit ($x = a, b, c$). (a) "P," $i_x > 0\,[S_x = 0]$. (b) "O," $i_x > 0\,[S_x = 1]$. (c) "O," $i_x < 0\,[S_x = 1]$. (d) "N," $i_x < 0\,[S_x = 0]$.

This paper is organized as follows. In Section II, operational characteristics and average model of the Vienna rectifier under unbalanced dc-link voltages are presented. In a slant and asymmetrical space vector diagram, the essential reason of current distortion is analyzed in detail. In Section III, a novel zero-sequence component injection method of the Vienna rectifier for current harmonics mitigation is proposed. In Section IV, simulated and experimental results verify the performance of the proposed zero-sequence component injection method. Finally, conclusions are drawn in Section V.

II. Operation of the Vienna Rectifier

Fig. 1 shows the topology of the Vienna rectifier, which includes six diodes, three filter inductors, two capacitors, and three bidirectional switching units (S_a, S_b, and S_c). Three switching units are controlled to ensure sinusoidal ac current and steady dc-link voltage ($V_{\rm dc}$). V_1 and V_2 are expressed as the upper and lower capacitor voltages of the dc link, respectively.

A. Operational Characteristics of the Vienna Rectifier

The operational states of the Vienna rectifier are presented in Fig. 2. These are determined by not only the controlled switching unit but also the polarity of the ac phase current at a corresponding instance.

Assuming the three-phase grids are balanced, the grid voltage can be defined as e_a, e_b, and e_c

$$\begin{cases} e_a = V_m \cos\theta \\ e_b = V_m \cos(\theta - 2\pi/3) \\ e_c = V_m \cos(\theta + 2\pi/3) \end{cases} \tag{1}$$

where V_m and θ are the amplitude and phase angle of grid voltages. When the Vienna rectifier operates with the unity power factor, the grid currents (i_x, $x = a, b, c$) can be expressed by

$$\begin{cases} i_a = I_m \cos(\theta) \\ i_b = I_m \cos(\theta - 2\pi/3) \\ i_c = I_m \cos(\theta + 2\pi/3) \end{cases} \tag{2}$$

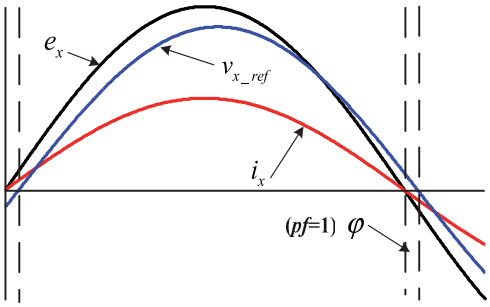

Fig. 3. Vienna rectifier operation when pf = 1.

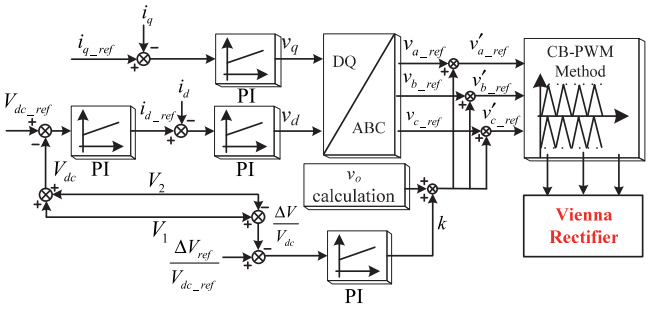

Fig. 4. Control block diagram of the Vienna rectifier with the traditional zero-sequence injection method.

TABLE I
LAGGING PHASE ANGLE ACCORDING TO CURRENTS AND REFERENCE VOLTAGES POLARITY

Sector	Currents polarity	Subsector	Reference voltages polarity	θ
I	(+, –, –)	1	(+, –, +)	[–π/6, φ – π/6]
		2	(+, –, –)	[φ – π/6, π/6]
II	(+, +, –)	3	(+, –, –)	[π/6, π/6 + φ]
		4	(+, +, –)	[π/6 + φ, π/2]
III	(–, +, –)	5	(+, +, –)	[π/2, π/2 + φ]
		6	(–, +, –)	[π/2 + φ, 5π/6]
IV	(–, +, +)	7	(–, +, –)	[5π/6, 5π/6 + φ]
		8	(–, +, +)	[5π/6 + φ, 7π/6]
V	(–, –, +)	9	(–, +, +)	[7π/6, 7π/6 + φ]
		10	(–, –, +)	[7π/6 + φ, 3π/2]
VI	(+, –, +)	11	(–, –, +)	[3π/2, 3π/2 + φ]
		12	(+, –, +)	[3π/2 + φ, –π/6]

where I_m is the amplitude of the phase input current. Due to the filter impedance, the three-phase reference signals (v_{a_ref}, v_{b_ref}, v_{c_ref}) are expressed as

$$\begin{cases} v_{a\_ref} = m\cos(\theta - \varphi) \\ v_{b\_ref} = m\cos(\theta - 2\pi/3 - \varphi) \\ v_{c\_ref} = m\cos(\theta + 2\pi/3 - \varphi) \end{cases} \tag{3}$$

where m is the modulation index, θ is the phase angle, and φ is the lagging angle. The input waveforms and reference signal are shown in Fig. 3 when the Vienna rectifier operates with a unity power factor (pf = 1).

As shown in Fig. 1, when $i_x > 0$, the voltage between points x and o (u_{xo}, $x = a, b, c$) consist of V_1 and zero; otherwise, u_{xo} consists of $–V_2$ and zero. This divides the space vector diagram into six vector sectors (I, II, III, IV, V, VI). Meanwhile, lagging angle φ exists in each vector sector. Hence, 12 subsectors and corresponding phase angle follow the rules in Table I. Additionally, it is known that the lagging angle φ cannot exceed 30°, which is the maximum phase allowed between the current and the voltage [12].

B. Average Model of the Vienna Rectifier With Unbalanced DC-Link Voltages

Considering the unbalanced dc-link voltages, the dc-link voltage V_{dc} is expressed as

$$V_{dc} = V_1 + V_2. \tag{4}$$

The difference voltage ΔV between upper and lower voltage is denoted as

$$\Delta V = V_1 - V_2. \tag{5}$$

The voltage unbalanced factor k ($–1 < k < 1$) is defined as

$$k = \frac{V_1 - V_2}{V_1 + V_2}. \tag{6}$$

For each phase loop, the Kirchhoff voltage law equations are expressed as

$$\begin{cases} e_a - L\frac{di_a}{dt} = u_{ao} + u_{on} = \frac{V_{dc}}{2}\cdot v_{a\_ref} \\ e_b - L\frac{di_b}{dt} = u_{bo} + u_{on} = \frac{V_{dc}}{2}\cdot v_{b\_ref} \\ e_c - L\frac{di_a}{dt} = u_{co} + u_{on} = \frac{V_{dc}}{2}\cdot v_{c\_ref} \end{cases} \tag{7}$$

where u_{on} is the common mode voltage

$$\begin{cases} e_d = L\frac{di_d}{dt} - \theta L i_q + \frac{V_{dc}}{2} v_{d\_ref} \\ e_q = L\frac{di_q}{dt} + \theta L i_d + \frac{V_{dc}}{2} v_{q\_ref}. \end{cases} \tag{8}$$

Based on (8), the controller of the Vienna rectifier is designed based on the synchronous reference frame (*d–q* frame). To extend the available modulation range to 1.15, the zero-sequence component v_o is injected into the three-phase reference signals v_{x_ref} ($x = a, b, c$). The modified reference signals denoted as v'_{x_ref} ($x = a, b, c$) can be expressed as

$$\begin{cases} v'_{a\_ref} = v_{a\_ref} + v_o \\ v'_{b\_ref} = v_{b\_ref} + v_o \\ v'_{c\_ref} = v_{c\_ref} + v_o \end{cases} \tag{9}$$

$$v_o = -\frac{f_{max} + f_{min}}{2} \tag{10}$$

where f_{max} and f_{min} are defined as

$$\begin{cases} f_{max} = \max(v_{a\_ref}, v_{b\_ref}, v_{c\_ref}) \\ f_{min} = \min(v_{a\_ref}, v_{b\_ref}, v_{c\_ref}). \end{cases} \tag{11}$$

The injected zero-sequence component can be modified as follows when considering the unbalanced factor:

$$v'_o = -\frac{f_{max} + f_{min}}{2} + k. \tag{12}$$

According to the average model of the Vienna rectifier in (8)–(12), Fig. 4 shows the total block diagram of the traditional control and zero-sequence component injection method, as well as the NP potential control strategy for the Vienna rectifier.

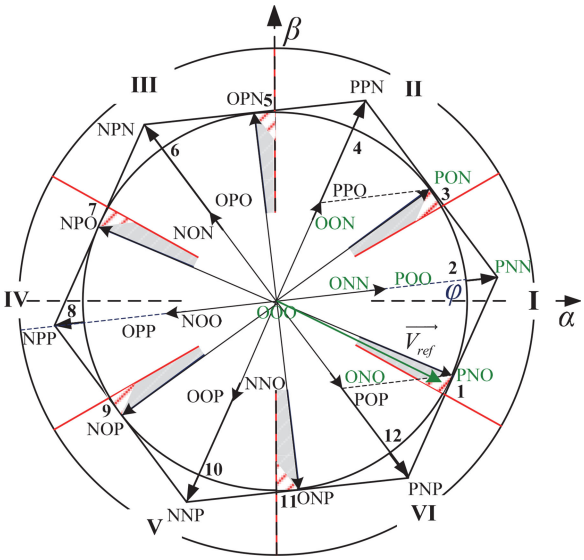

Fig. 5. Slant space vector diagram of the Vienna rectifier with $k = 0$.

On the base of a balancing mechanism, the variable of the zero-sequence component (Δv_o) is able to regulate the potential voltage at a neutral point. As the variable of the zero-sequence component shown in Fig. 4, the unbalanced factor is added to the zero-sequence component (v_o). In addition, k is obtained through feedback of the output voltage difference (Δv) with a PI controller. Balanced dc-link voltage is only a special case of unbalance when $k = 0$. Therefore, balanced and unbalanced dc-link voltages are controlled accurately by changing $\Delta V_{\text{ref}}/V_{\text{dc\_ref}}$ in application of electric vehicle charging station or energy storage station.

C. Current Distortion Analysis

The main drawback of the traditional zero-sequence injection method is the input current distortion caused by the inherent topological characteristics of the Vienna rectifier. To analyze current distortion directly, the switching states with the space vector diagram are illustrated in two operation modes: 1) $k = 0$; and 2) $k \neq 0$.

The space vector diagram under the first mode is presented in Fig. 5, where the space voltage vectors can be divided into four groups: zero, small, medium, and large vector, as listed in Table II.

Because of the force commutated current, lagging angle (φ) slants the space vector diagram of the Vienna rectifier, as shown in Fig. 5. Hence, only eight green coordinate vectors can be used as the candidates when the voltage reference vector ($\overrightarrow{V_{\text{ref}}}$) locates in the red shadow zones in subsector 1. The hexagon, which is composed of [OOO], [OON], [PON], [PNN], [PNO], [ONO], [ONN], and [POO], cannot cover the red shadow zone. As a result, $\overrightarrow{V_{\text{ref}}}$ is not properly synthesized. This is the main reason of current distortion for the Vienna rectifier with balanced dc-link voltages especially at the zero-crossing point.

Considering the second mode, the revised space voltage vector diagrams are slant and asymmetrical, as shown in Fig. 6. It

TABLE II
VOLTAGE VECTORS AND CORRESPONDING SWITCHING STATES

Vector	Magnitude	Switching state	
Zero vector	0	[PPP] [OOO] [NNN]	
Small vector	$\frac{1}{3}V_{\text{dc}}$	P-type	N-type
		[POO]	[ONN]
		[PPO]	[OON]
		[OPO]	[NON]
		[OPP]	[NOO]
		[POP]	[ONO]
		[OOP]	[NNO]
Medium vector	$\frac{\sqrt{3}}{3}V_{\text{dc}}$	[PON] [OPN] [NPO] [NOP] [ONP] [PNO]	
Large vector	$\frac{2}{3}V_{\text{dc}}$	[PNN] [PPN] [NPN] [NPP] [NNP] [PNP]	

can be seen that six pairs of small vectors are not overlapped anymore and the medium vectors deviate from their original locations. Zero vectors and large vectors are not affected by the unbalanced dc-link voltages.

For the case that $0 < k < 1$, the reference vector ($\overrightarrow{V_{\text{ref}}}$) locates in sector I. As shown in Fig. 6(a), the area of hexagon is smaller than it in the case of $k = 0$. Thus, two orange zones appear accordingly in which reference vector $\overrightarrow{V_{\text{ref}}}$ is not synthesized using the traditional zero-sequence injection method. It is convenient to combine the red shadow zone in subsector 1 and the orange zone in subsector 2 as the P_A state and define the other orange zone in subsector 2 as the P_B state. Six P states appear at the same time when $0 < k < 1$, as shown in Fig. 6(a). For another case that $-1 < k < 0$, the same analysis can be elaborated. In a similar way, six N states appear simultaneously in Fig. 6(b). Hence, $\overrightarrow{V_{\text{ref}}}$ cannot be synthesized by relevant switching states if the reference vector locates in these P states and N states, which are defined as abnormal regions. Therefore, abnormal regions are the essential reason of severe current distortion for the Vienna rectifier. Obviously, the lagging angle and absolute value of the unbalanced factor would increase the size of abnormal regions when $k \neq 0$. So comparing with the balanced mode, the current distortion is even worse when dc-link voltages are unbalanced. Furthermore, because of force commutated current, [POP] and [PNP] are disabled as synthesized vectors in Fig. 6(a). Therefore, a simplified PWM strategy proposed in [27], which utilizes [POP] or [PPO] as nearest vectors to extend the linear modulation range, is improper for the Vienna rectifier. To solve this problem, a novel zero-sequence component injection method is proposed in this paper.

III. Proposed Zero-Sequence Component Injection Method for Current Harmonic Mitigation

Based on the previous analysis, both lagging angle and unbalanced factor can lead to the current distortion. The proposed zero-sequence component injection method could compensate the effect of lagging angle and unbalanced factor by assuming two main calculation steps: 1) identification of abnormal regions in a simple way and 2) calculation of compensation components.

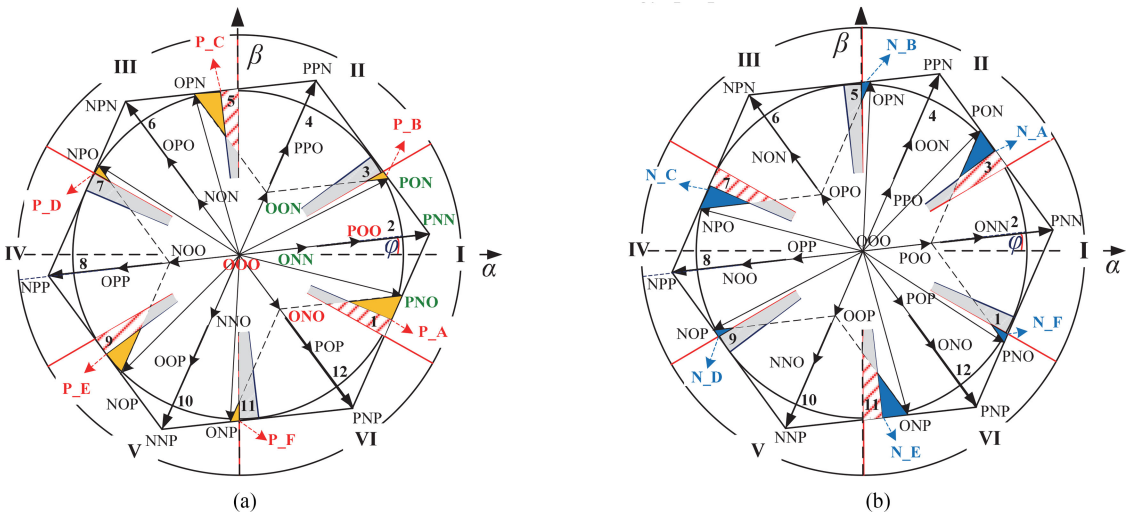

Fig. 6. Asymmetrical space vector diagrams of the Vienna rectifier with $k \neq 0$. (a) $0 < k < 1$. (b) $-1 < k < 0$.

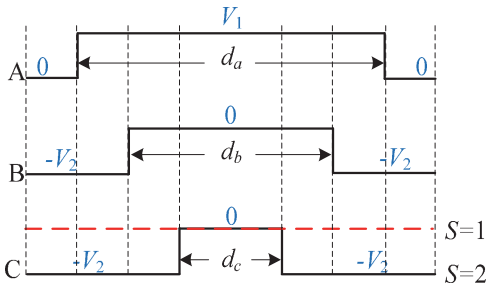

Fig. 7. Relationship between average duties and switching sequences for the Vienna rectifier in sector I.

A. *Identification of Abnormal Regions*

A single CB-PWM switching method is implemented for switching the semiconductor devices easily. For this section, sector I is taken as an example to analyze the zero-sequence injection method in detail. The average duties are defined as d_x $(x = a, b, c)$ shown in Fig. 7 when the reference vector locates in sector I.

When $i_a > 0, i_b < 0, i_c < 0, u_{xo}$ $(x = a, b, c)$ are determined by average duties as

$$\begin{cases} u_{ao} = \frac{V_{dc}}{2} \cdot (v_{a\_ref} + v'_o) = \frac{V_{dc}}{2} \cdot (1+k) \cdot d_a \\ u_{bo} = \frac{V_{dc}}{2} \cdot (v_{b\_ref} + v'_o) = -\frac{V_{dc}}{2} \cdot (1-k) \cdot (1-d_b) \\ u_{co} = \frac{V_{dc}}{2} \cdot (v_{c\_ref} + v'_o) = -\frac{V_{dc}}{2} \cdot (1-k) \cdot (1-d_c). \end{cases} \tag{13}$$

In general, three-phase duty equations can be calculated by

$$\begin{cases} d_a = \frac{v_{a\_ref} + v_o + k}{1+k} \\ d_b = 1 + \frac{v_{b\_ref} + v_o + k}{1-k} \\ d_c = 1 + \frac{v_{c\_ref} + v_o + k}{1-k}. \end{cases} \tag{14}$$

With (3), (9), (10), and (11), three-phase reference signals $(v'_{x\_ref}, x = a, b, c)$ can be obtained after zero-sequence injection according to θ. When $-\pi/6 \le \theta \le \varphi$, v'_{a_ref}, v'_{b_ref}, v'_{c_ref} are expressed by

$$\begin{cases} v'_{a\_ref} = -(\sqrt{3}/2)m \sin\left(\theta - \frac{\pi}{3} - \varphi\right) \\ v'_{b\_ref} = (\sqrt{3}/2)m \sin\left(\theta - \frac{\pi}{3} - \varphi\right) \\ v'_{c\_ref} = (3/2)m \cos\left(\theta + \frac{2\pi}{3} - \varphi\right). \end{cases} \tag{15}$$

By means of trigonometric functions, the extreme values of (15) are obtained as

$$\begin{cases} (3/4)m \le v'_{a\_ref} \le (\sqrt{3}/2)m \\ -(\sqrt{3}/2)m \le v'_{b\_ref} \le -(3/4)m \\ -(3/4)m \le v'_{c\_ref} \le (3/2)m \sin\varphi. \end{cases} \tag{16}$$

After substituting (14) into (16), the inequalities of the average duty can be given by

$$\begin{cases} \frac{(3/4)m+k}{1+k} \le d_a \le \frac{(\sqrt{3}/2)m+k}{1+k} \\ \frac{-(\sqrt{3}/2)m+k}{1-k} + 1 \le d_b \le \frac{-(3/4)m+k}{1-k} + 1 \\ \frac{-(3/4)m+k}{1-k} + 1 \le d_c \le \frac{(3/2)m\sin\varphi+k}{1-k} + 1. \end{cases} \tag{17}$$

Owing to φ and k, average duties in inequalities (17) could be driven out of [0, 1] when abnormal intervals appear. Therefore, to ensure the normal operation of the Vienna rectifier, the following constraint should be met for (17) (refer to the Appendix for details):

$$|k| \le \frac{3}{4}m. \tag{18}$$

Different from d_a and d_b, an additional constraint given as follows for d_c should be met at the same time:

$$k \le -\frac{3}{2}m \sin\varphi. \tag{19}$$

When $\varphi \le \theta \le \pi/6$, v'_{a_ref}, v'_{b_ref}, and v'_{c_ref} are expressed by

$$\begin{cases} v'_{a\_ref} = (\sqrt{3}/2)m \sin\left(\theta + \frac{\pi}{3} - \varphi\right) \\ v'_{b\_ref} = (3/2)m \cos\left(\theta - \frac{2\pi}{3} - \varphi\right) \\ v'_{c\_ref} = -(\sqrt{3}/2)m \sin\left(\theta + \frac{\pi}{3} - \varphi\right). \end{cases} \tag{20}$$

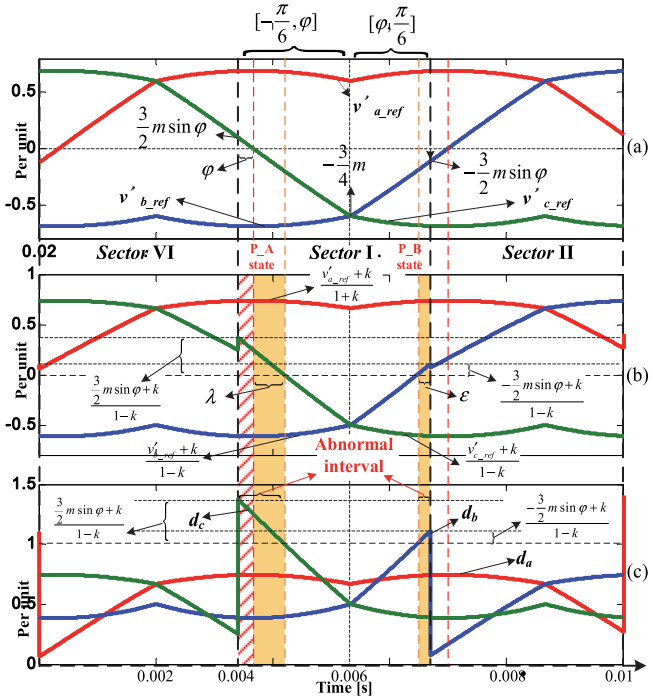

Fig. 8. Mechanism of abnormal intervals for identification in sector I when $m = 0.8$ and $\varphi = 6°$. (a) Three-phase reference signals before modification of k. (b) Three-phase reference signals after modification of k. (c) Average duties with identification of abnormal intervals.

Depending on the same algebraic manipulation, the extreme values of (20) are obtained as

$$\begin{cases} \frac{3}{4}m \le v'_{a\_\mathrm{ref}} \le \frac{\sqrt{3}}{2}m\cos\varphi \\ -\frac{3}{4}m \le v'_{b\_\mathrm{ref}} \le \frac{3}{2}m\sin\varphi \\ -\frac{\sqrt{3}}{2}m\cos\varphi \le v'_{c\_\mathrm{ref}} \le -\frac{3}{4}m. \end{cases} \tag{21}$$

After substituting (20) into (21), the inequalities of the average duty can be given by

$$\begin{cases} \frac{(3/4)m+k}{1+k} \le d_a \le \frac{(\sqrt{3}/2)m\cos\varphi+k}{1+k} \\ \frac{-(3/4)m+k}{1-k}+1 \le d_b \le \frac{(3/2)m\sin\varphi+k}{1-k}+1 \\ \frac{-(\sqrt{3}/2)m\cos\varphi+k}{1-k}+1 \le d_c \le \frac{-(3/4)m+k}{1-k}+1. \end{cases} \tag{22}$$

Comparing with the situation of $-\pi/6 \le \theta \le \varphi$, an additional constraint given as follows for d_b should be met by adopting the similar method as presented in the Appendix:

$$k \ge \frac{3}{2}m\sin\varphi. \tag{23}$$

For the operation of the Vienna rectifier, m and k should agree with the requirement of (18) always. When breaking the additional constraints (19) and (23), the identification of abnormal intervals is only based on d_c and d_b in sector I. For example, three-phase reference signals (v'_{a_ref}, v'_{b_ref}, v'_{c_ref}) before and after modification of k (0.2) are shown in Fig. 8(a) and (b) when $m = 0.8$ and $\varphi = 6°$. The average duties calculated by (13) are presented in Fig. 8(c).

Assuming the angle of the reference vector during the P_A state caused by k is denoted as λ in the interval of an orange block in Fig. 8. θ including φ and λ can be calculated by (24)

TABLE III
THREE-PHASE DUTY EQUATIONS FOR EACH SECTOR

Sector	Duty equations	Sector	Duty equations
I	$\begin{cases} d_a = \frac{v_{a\_\mathrm{ref}}+v_o+k}{1+k} \\ d_b = 1+\frac{v_{b\_\mathrm{ref}}+v_o+k}{1-k} \\ d_c = 1+\frac{v_{c\_\mathrm{ref}}+v_o+k}{1-k} \end{cases}$	IV	$\begin{cases} d_a = 1+\frac{v_{a\_\mathrm{ref}}+v_o+k}{1-k} \\ d_b = \frac{v_{b\_\mathrm{ref}}+v_o+k}{1+k} \\ d_c = \frac{v_{c\_\mathrm{ref}}+v_o+k}{1+k} \end{cases}$
II	$\begin{cases} d_a = \frac{v_{a\_\mathrm{ref}}+v_o+k}{1+k} \\ d_b = \frac{v_{b\_\mathrm{ref}}+v_o+k}{1+k} \\ d_c = 1+\frac{v_{c\_\mathrm{ref}}+v_o+k}{1-k} \end{cases}$	V	$\begin{cases} d_a = 1+\frac{v_{a\_\mathrm{ref}}+v_o+k}{1-k} \\ d_b = 1+\frac{v_{b\_\mathrm{ref}}+v_o+k}{1-k} \\ d_c = \frac{v_{c\_\mathrm{ref}}+v_o+k}{1+k} \end{cases}$
III	$\begin{cases} d_a = 1+\frac{v_{a\_\mathrm{ref}}+v_o+k}{1-k} \\ d_b = \frac{v_{b\_\mathrm{ref}}+v_o+k}{1+k} \\ d_c = 1+\frac{v_{c\_\mathrm{ref}}+v_o+k}{1-k} \end{cases}$	VI	$\begin{cases} d_a = \frac{v_{a\_\mathrm{ref}}+v_o+k}{1+k} \\ d_b = 1+\frac{v_{b\_\mathrm{ref}}+v_o+k}{1-k} \\ d_c = \frac{v_{c\_\mathrm{ref}}+v_o+k}{1+k} \end{cases}$

when $(v'_{c\_\mathrm{ref}}+k)/(1-k) = 0$. Thus, λ in the interval of the orange block is given by (25) as follows:

$$\frac{\frac{3}{2}m\cos\left(\theta+\frac{2\pi}{3}-\varphi\right)+k}{1-k} = 0 \tag{24}$$

$$\lambda = \theta-\varphi = \arccos\left(-\frac{2k}{3m}\right)-\frac{2\pi}{3}. \tag{25}$$

Similarly, the angle of the reference vector during the P_B state is denoted as ε. It illustrates the difference between $\pi/6$ and θ. θ can be calculated by (26) when $(v'_{b\_\mathrm{ref}}+k)/(1-k) = 0$. Therefore, ε in the interval of the orange block named the P_B state is given by (27) as follows:

$$\frac{\frac{3}{2}m\cos\left(\theta-\frac{2\pi}{3}-\varphi\right)+k}{1-k} = 0 \tag{26}$$

$$\varepsilon = \frac{\pi}{6}-\theta = -\arccos\left(-\frac{2k}{3m}\right)-\frac{\pi}{2}-\varphi. \tag{27}$$

Based on distinguishing abnormal intervals caused by φ and k, identification leads to complicated online calculations of trigonometric functions. However, the abnormal intervals are unchanged by duty equations, as shown in Fig. 8(b) and (c). Comparing d_c and d_b calculated by (13) with 1, it is an easy way to identify the abnormal intervals in sector I. The above-mentioned analysis can be also extended to the other sectors. The three-phase duty equations for all six sectors are listed in Table III.

To illustrate the validity of analysis for abnormal intervals, the average duties and actual reference signals under the influence of different unbalanced factors are illustrated in Figs. 9 and 10. For example, when $m = 0.8$, $\varphi = 6°$, the range of k must meet the following $-0.6 < k < 0.6$ according to constraint (18). The range of k is divided into three parts including [–0.6, –0.12], [–0.12, 0.12], and [0.12, 0.6] according to the constraints (19) and (23).

When k located in the range of [–0.12, 0.12] is equal to zero, the average duties and actual reference signals are presented in the top and bottom of Fig. 9, respectively. Obviously, six abnormal intervals including three P states and three N states appear. In detail, d_c is forced to be 1 due to lagging angle φ

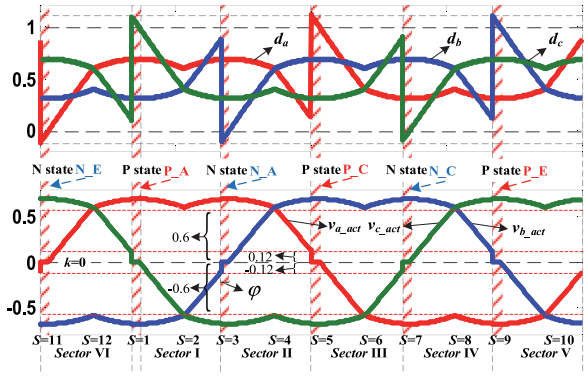

Fig. 9. Average duties and actual reference signals with $k = 0$.

in subsector 1. For the same reason, d_b is forced to be 0 in subsector 3.

When $k \neq 0$, in the case of $k = 0.05$, k is in the range of [–0.12, 0.12]. As shown in Fig. 10(a), three P states and three N states still exist in every sector interval as the same as the situation when $k = 0$. Three abnormal intervals denoted as P states are increased by the orange interval, while the other three abnormal intervals (N states) are decreased comparing the abnormal intervals (N states) in Fig. 9. In detail, d_c is forced to be 1 because $k = 0.05$ and $\varphi = 6°$. In the adverse case, as shown in Fig. 10(b), three abnormal intervals denoted as N states are increased by blue shadows, while the other three abnormal intervals (P states) are decreased. As a result, the identification of abnormal intervals in these two cases is easy by comparing d_c with 1 in sector I.

As the degree of unbalanced dc-link voltages increases, another two different situations are shown in Fig. 10(c) and (d). In the case of $k = 0.2$, k is in the range of [0.12, 0.6]. Comparing with Fig. 10(a), it can be seen that six P states without N states exist. With the increase of k, the abnormal interval in sector II disappears. However, an additional abnormal interval defined as the P_B state comes out in sector I except for the P_A state. It means that additional constraint (22) is unsatisfied when $k = 0.2$. The appearance of the P_B state is the same as the analysis in slant and asymmetrical space vector diagrams. For this situation, the abnormal intervals should be identified by results of $d_c > 1$ and $d_b > 1$ simultaneously in sector I. In an opposing case presented in Fig. 10(d), six N states without P states exist when $k = –0.2$. The abnormal intervals should be identified by results of $d_b < 0$ and $d_a < 0$ simultaneously in sector II. As a result, this identification contains all situations shown in Figs. 9 and 10. In addition, the application of this identification is easy without detecting the position of the reference vector in the slant and asymmetrical space vector diagrams to reduce the calculation time.

B. Calculation of Compensation Components

After average duties limitation, one of three-phase actual reference waveforms shown in Fig. 10 is clamped to zero in abnormal intervals. It can be seen that information of the reference vector is incomplete, which is the main reason of current distortion. Nevertheless, average duties can be manipulated handily after identification of abnormal intervals as established earlier. For instance, when $0 < k < 1$ in sector I, the average duty d_c, which is clamped to 1 during the P_A state, can be unchanged owing to the operational requirement of the Vienna rectifier. It means that the compensation component d_{c_com} obtained by the following equation is added to d_c in the abnormal interval:

$$d_{c\_com} = -(d_c - 1). \tag{28}$$

Using the proposed zero-sequence component injection method, other two compensation components d_{a_com} and d_{b_com} should be added to d_a and d_b correspondingly. In view of the space vector diagram, only [OOO], [POO], and [ONO] can be used to synthesize the output voltage vector when the reference vector $\overrightarrow{V_{\text{ref}}}$ locates in the P_A state. Therefore, the three-phase modified average duties (D_a, d_b, and d_c) for the Vienna rectifier are expressed as

$$\begin{cases} D_a = d_a + d_{a\_com} \\ D_b = d_b + d_{b\_com} \\ D_c = d_c + d_{c\_com}. \end{cases} \tag{29}$$

Based on the injection mechanism of the zero-sequence component, three components should be the same when $k = 0$ in sector I. It is worth highlighting that d_{a_com}, d_{b_com}, and d_{c_com} are not equal to each other because the dc-link voltage is unbalanced. The compensation component d_{b_com} expressed by the following equation is equal to d_{c_com} when reference signals have the same signs in the P state:

$$d_{b\_com} = -(d_c - 1). \tag{30}$$

When the signs of reference signals are different, d_{a_com} can be calculated by the following equation without breaking the volt-second balance principle by appropriately adjusting a transformation coefficient

$$d_{a\_com} = -(d_c - 1)\frac{1-k}{1+k}. \tag{31}$$

In the other way, calculation of compensation components needs a reciprocal coefficient in N states. For the convenience of analysis, T_1 and T_2 obtained by the following equations are defined as transformation coefficients for P states and N states, respectively

$$T_1 = \frac{1-k}{1+k} \tag{32}$$

$$T_2 = \frac{1+k}{1-k}. \tag{33}$$

Depending on the unbalanced factor, three compensation components are calculated in real time. Theoretically, the proposed method has more accurate performance in steady or transient states regardless of balanced or unbalanced dc-link voltages. In the proposed zero-sequence component injection method, the identifications of abnormal intervals and compensation components for all regions are listed in Table IV.

For example, three compensation components (d_{a_com}, d_{b_com}, and d_{c_com}) and actual reference signals after compensations (v'_{a_act}, v'_{b_act}, and v'_{c_act}) are shown in Fig. 11. Six P states can be identified in Fig. 11(a) using the proposed method

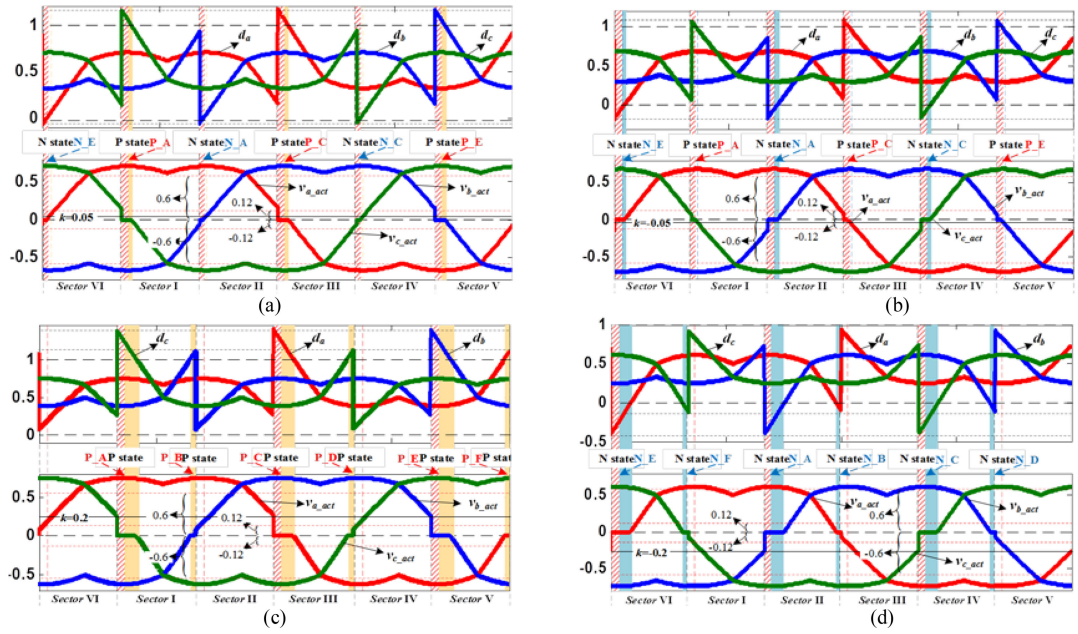

Fig. 10. Average duties and actual reference signals with lagging phase angle $\varphi = 6^\circ$ for (a) $k = 0.05$, (b) $k = -0.05$, (c) $k = 0.2$, and (d) $k = -0.2$.

TABLE IV
IDENTIFICATION OF ABNORMAL INTERVAL AND COMPENSATION COMPONENTS

Sector	Compensating condition	Region	dx_com	Compensation Component
I	$d_c > 1$	P_A	d_a_com	$-(d_c-1)^*T_1$
			d_b_com	$-(d_c-1)$
			d_c_com	$-(d_c-1)$
	$d_b > 1$	P_B	d_a_com	$-(d_b-1)^*T_1$
			d_b_com	$-(d_b-1)$
			d_c_com	$-(d_b-1)$
II	$d_b < 0$	N_A	d_a_com	$-d_b$
			d_b_com	$-d_b$
			d_c_com	$d_b^*T_2$
	$d_a < 0$	N_B	d_a_com	$-d_a$
			d_b_com	$-d_a$
			d_c_com	$-d_a^*T_2$
III	$d_a > 1$	P_C	d_a_com	$-(d_a-1)$
			d_b_com	$-(d_a-1)^*T_1$
			d_c_com	$-(d_a-1)$
	$d_c > 1$	P_D	d_a_com	$-(d_c-1)$
			d_b_com	$-(d_c-1)^*T_1$
			d_c_com	$-(d_c-1)$
IV	$d_c < 0$	N_C	d_a_com	$-d_c^*T_2$
			d_b_com	$-d_c$
			d_c_com	$-d_c$
	$d_b < 0$	N_D	d_a_com	$-d_b^*T_2$
			d_b_com	$-d_b$
			d_c_com	$-d_b$
V	$d_b > 1$	P_E	d_a_com	$-(d_b-1)$
			d_b_com	$-(d_b-1)$
			d_c_com	$-(d_b-1)^*T_1$
	$d_a > 1$	P_F	d_a_com	$-(d_a-1)$
			d_b_com	$-(d_a-1)$
			d_c_com	$(d_a-1)^*T_1$
VI	$d_a < 0$	N_E	d_a_com	$-d_a$
			d_b_com	$d_a{}^*T_2$
			d_c_com	$-d_a$
	$d_c < 0$	N_F	d_a_com	$-d_c$
			d_b_com	$-d_c^*T_2$
			d_c_com	$-d_c$

when $m = 0.8$ and $k = 0.2$. On the contrary, six N states are presented in Fig. 11(b) using the proposed method when $k = -0.2$. In another way, only three P states and three N states appear if the absolute value of the unbalanced factor k reduces to 0.05 in Fig. 11(c). Comparing three compensation components (d_{a_com}, d_{b_com}, and d_{c_com}) in the top of Fig. 11(a) at 0.004 s, d_{a_com} is smaller than d_{b_com} during the P_A state. Likewise, the three-phase compensation components are unequal to each other during other five P states. In the opposing case, T_2 is applied to calculate compensation components during N states.

After compensations, three average duties are modified in the abnormal interval to meet the operational requirements of Vienna rectifier and volt-second balance principle based on the injection mechanism of the zero-sequence component. Depending on the actual reference signals shown in the bottom of Fig. 11, the achievable condition of adding compensation components to the three-phase average duties is that there must be enough headroom. It is a compromise between compensation and modulation range, which is used to reduce the dc-link voltage.

On this account, the high dc-link voltage utilization is the main limitation for practical applications. The entire block diagram of the proposed zero-sequence component injection method of the Vienna rectifier for current harmonic mitigation is shown in Fig. 12.

Being different from the traditional zero-sequence component injection method in Fig. 4, gray blocks in Fig. 12 identify the abnormal interval and add compensation components to average duties. The range of the abnormal interval and the values of compensation components are calculated in real time. After that, the switching signals are obtained by a single carrier to drive the bidirectional switches. As a nongenerative-boost type rectifier, the Vienna rectifier is commonly used in a dc power supply system including ac–dc and buck-type dc–dc stage (which is mainly seen in on-board or off-board charger for the electric

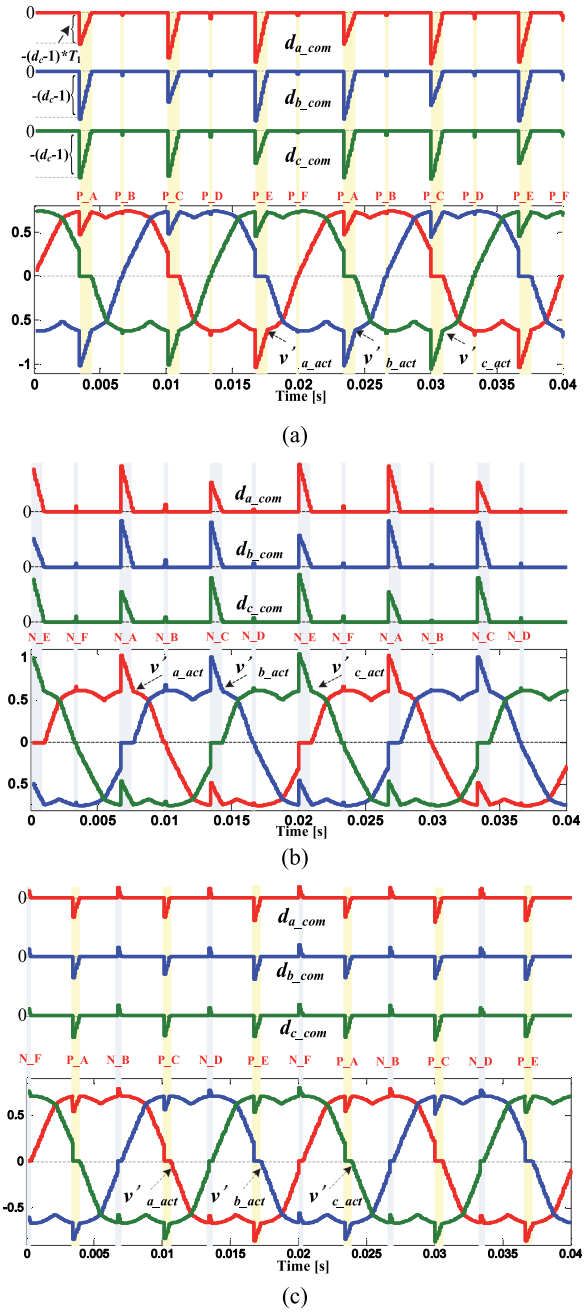

Fig. 11. Three-phase compensation components and actual reference signals using the proposed method with $m = 0.8$. (a) $k = 0.2$. (b) $k = -0.2$. (c) $k = 0.05$.

vehicle). In this case, the dc-link voltage could be set at a higher voltage level. Furthermore, using the zero-sequence component injection modulation, the available modulation range is extended to 1.15. As a result, the proposed method keeps more margin of headroom for the compensation component.

IV. Simulation and Experimental Results

To verify the performance of the proposed zero-sequence component injection method, both simulations and experiments are conducted to compare with two types of traditional methods. For the one type, the zero-sequence component injection modulation method bases on the unbalanced factor without compensations, which is denoted as traditional method 1. For the other type, traditional method 2 proposed in the literature [12] contains compensations neglecting the unbalanced factor. The parameters for the simulation and experiment in this paper are shown in Table V.

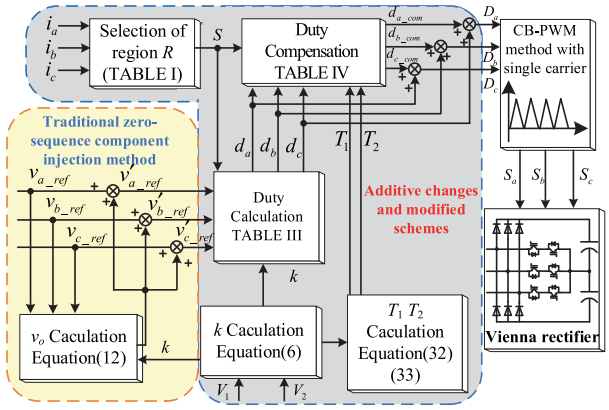

Fig. 12. Block diagram of the proposed zero-sequence component injection method of the Vienna rectifier.

TABLE V
Parameters for Simulation and Experiment

Parameter	Simulation values	Experiment values
Line voltage e_{ab}, e_{bc}, e_{ca}	380 V [rms]	380 V [rms]
DC-link voltage	700 V	700 V
DC-link capacitor	3300 μF	2200 μF
DC loads	$R_1 = R_2 = 35\ \Omega$	$R_1 = R_2 = 50\ \Omega$
Peak current	20 A	9 A
L-filter	6 mH	3 mH
Switching frequency	10 kHz	10 kHz
Sampling time T_s	100 μs	100 μs

A. Simulation Results Analysis

In the simulation, the Vienna rectifier works with dual dc loads using the traditional zero-sequence component injection method. Its simulation waveforms of line voltage, two dc-link voltages, input currents, and dc loads currents are shown in Fig. 13.

At first, two balanced dc-link voltages are controlled ($V_1 = V_2 = 350$ V) during the range of time [0, 0.04 s] in Fig. 13(a) and (b). It can be seen that light distortions of current appear around the zero-crossing point. When two unbalanced dc-link voltages ($V_1 = 400$ V, $V_2 = 300$ V) are controlled during the range of time [0.04 s, 0.08 s], the currents are distorted even worse in the abnormal interval in Fig. 13(a). The input currents are disturbed in the corresponding opposing abnormal interval. Current distortions exist in the operation of the Vienna rectifier using traditional method 1 when dc-link voltages are balanced and unbalanced. Using traditional method 2, two unbalanced dc-link voltages ($V_1 = 400$ V, $V_2 = 300$ V) are controlled during the range of time [0.04 s, 0.08 s] as shown in Fig. 13(b). Though there are no current distortions using compensations

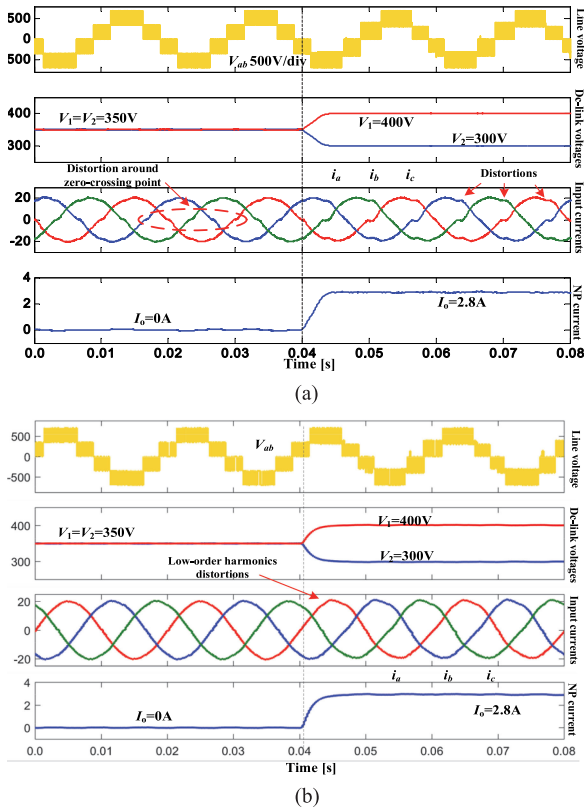

Fig. 13. Waveforms of the Vienna rectifier with dual dc loads using the traditional method from $k = 0$ to $0 < k < 1$. (a) Using traditional method 1. (b) Using traditional method 2.

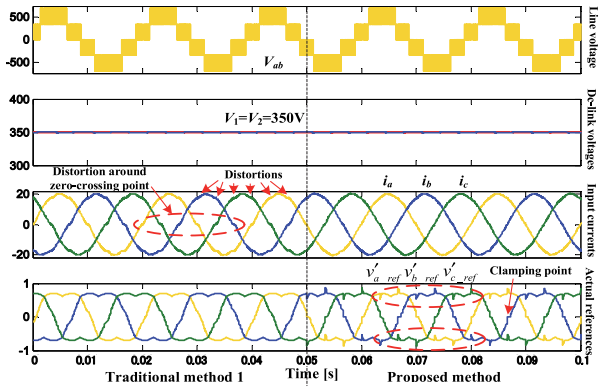

Fig. 14. Performance comparison of traditional method 1 and proposed method when dc-link voltages are balanced.

with balanced dc-link voltages, the input currents contain low-order harmonics when unbalanced dc-link voltages occur.

In order to suppress harmonics of input currents, a novel zero-sequence component injection method proposed in this paper is employed by modifying the average duty. Simulation waveforms of the harmonic mitigation are presented in Fig. 14 when two dc-link voltages are balanced.

Traditional zero-sequence component injection method 1 is used for the Vienna rectifier during simulation time [0, 0.05 s]. It is seen that distortions of input currents exist in every 60°, especially around zero-crossing points. The proposed zero-sequence component injection method is utilized in the simulation system during [0.05 s, 0.1 s]. Compensations are added to average duties for mitigating these distortions. Three-phase reference signals (v'_{a_ref}, v'_{b_ref}, v'_{c_ref}) using traditional method 1 and proposed zero-sequence component injection method are presented in Fig. 14. It can be seen that a reference signal is clamped to zero around the zero-crossing point and the other two are compensated in the abnormal interval using the proposed zero-sequence component injection method.

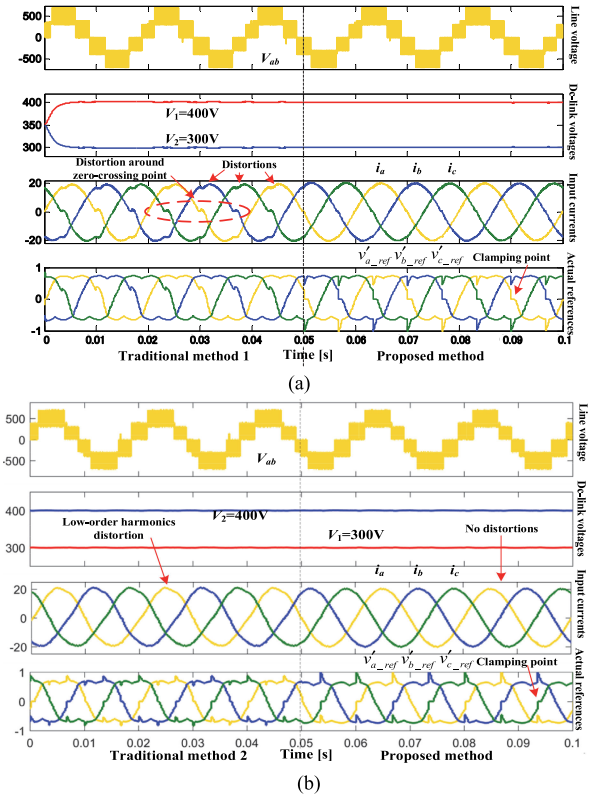

Fig. 15. Performance comparison of two traditional methods and proposed method when dc-link voltages are unbalanced. (a) V_1 is higher than V_2. (b) V_1 is lower than V_2.

The input currents are clean and sinusoidal in phase with the source voltages through adjusting the average duty. Total harmonic distortion (THD) of the input current for the Vienna rectifier decreases from 3.89% to 1.89% using the proposed zero-sequence component injection method. The performance of the proposed method is the same as that of traditional method 2 under the balanced dc-link voltages. However, traditional method 2 is incapable of handling the low-order harmonics distortion when the imbalance occurs. Therefore, simulations verify the performance of the proposed method comparing with two types of traditional methods in two cases where dc-link voltages are unequal, as shown in Fig. 15.

Case one: when V_1 (400 V) is higher than V_2 (300 V), the line voltage, input currents, and reference signals are shown in Fig. 15(a). Hence, unbalanced factor k is increased to 0.143. It is obvious that the input currents of the Vienna rectifier are seriously distorted around the zero-crossing point by the unbalanced factor using traditional method 1. The current THD is 10.02%. As stated previously, P states brought out input cur-

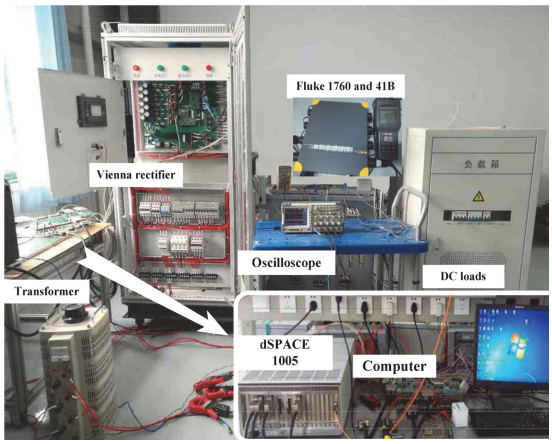

Fig. 16. Photograph of the experimental platform.

rent harmonic of the Vienna rectifier in sectors I, III, and V. Low harmonic (THD = 2.21%) can be achieved by applying the proposed zero-sequence component injection method during [0.05 s, 0.1 s] in Fig. 15(a).

Case two: when V_1 is lower than V_2 ($k = -0.14$), the comparison between traditional method 2 and proposed zero-sequence component injection method is presented in Fig. 15(b). It can be seen that input currents of the Vienna rectifier contain numerous low-order harmonics (mainly consisting of second- and fourth-order harmonics). As a result, the current THD is 6.7%. Using the proposed zero-sequence component injection method, the current distortions are mitigated significantly after 0.05 s. In the end, the current THD is 2.14% after improvement.

B. Experimental Results Verification

To verify the performance of the proposed method, experiments were performed in a prototype of T-type 3L converters, as shown in Fig. 16. In this experiment setup, the upper and lower switches for three phases in the T-type converter are OFF to operate as the Vienna rectifier. The power rating of the implemented system is 20 kVA. The key parameters for the experiment are shown in Table IV. The control system is dSPACE 1005 rapid prototyping kit.

Fig. 17 shows the experimental waveforms of the Vienna rectifier with traditional method 1 and proposed zero-sequence component injection method when dc-link voltages are balanced. The Vienna rectifier operates at unity power factor (pf). Its line voltage and input current behave as typical five voltage level waveform and sinusoidal waveform in Fig. 17(a) and (b). As shown in Fig. 17, the amplitudes of currents are about 9 A. Due to the filter impedance, it is obvious that there are some distortions of input currents around zero-crossing points. Comparing Fig. 17(c) and (d), the current distortions are eliminated significantly using the proposed zero-sequence component injection method.

Fig. 18 shows two dc-link voltages, one-phase actual reference signal, and input current of the Vienna rectifier when both two dc-link voltages are equal to 350 V. The phase current is distorted when the reference signal is not modified using the traditional zero-sequence component injection method. With the proposed method being employed, the reference signal is modified, as shown in Fig. 18(a), and the harmonic performance of the input current is improved distinctly. The actual reference signal is presented in detail in Fig. 18(b).

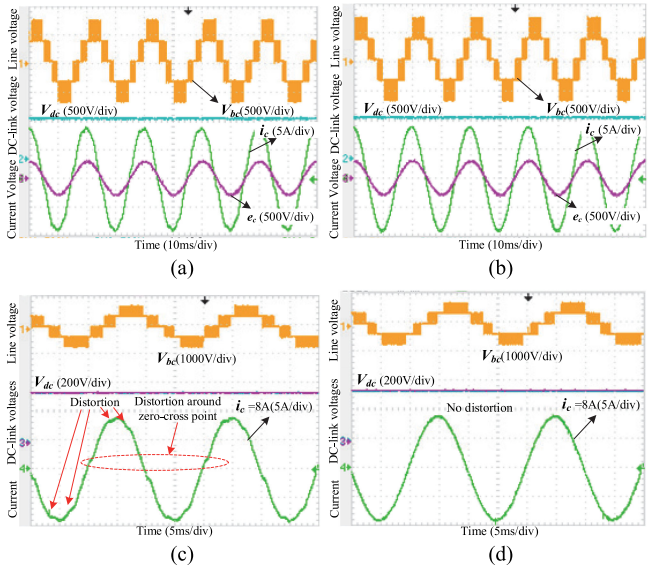

Fig. 17. Experiment waveforms of the Vienna rectifier when dc-link voltages are balanced. (a) Operation at a unity power factor using traditional method 1. (b) Operation at a unity power factor using the proposed method. (c) Distortion of the input current using traditional method 1. (d) No distortion of the input current using the proposed method.

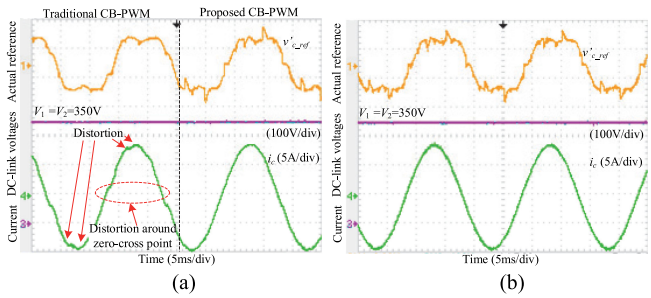

Fig. 18. Experiment waveforms when dc-link voltages are balanced $V_1 = V_2 = 350$ V. (a) Comparison between traditional method 1 and proposed method. (b) One-phase actual reference signal in detail.

Comparing with traditional method 1, Fig. 19 shows a comparison of the input phase currents and reference signal before and after the application of the proposed method. Similar to the simulation, unbalanced dc-link voltages are divided into two cases. Case one: the upper dc-link voltage ($V_1 = 380$ V or $V_1 = 425$ V) is higher than lower one ($V_2 = 320$ V or $V_2 = 275$ V). Case two: the upper dc-link voltage ($V_1 = 320$ V or $V_1 = 275$ V) is lower than the other ($V_2 = 380$ V or $V_2 = 425$ V). Fig. 19(a) shows the comparison in case one under a light imbalance. Fig. 19(b) shows the comparison in case one under a heavy imbalance. On the other case, the power quality of input currents is significantly improved, as shown in Fig. 19(c) and (d). Comparing the waveforms in two cases, the line voltage is adjusted

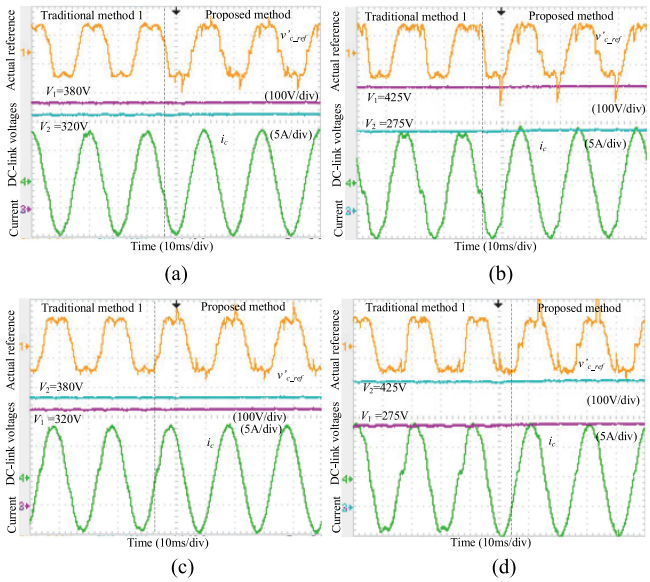

Fig. 19. Comparison of experiment results between traditional method 1 and proposed zero-sequence component injection method when two dc-link voltages are unbalanced. (a) Case one with a light imbalance. (b) Case one with a heavy imbalance. (c) Case two with a light imbalance. (d) Case two with a heavy imbalance.

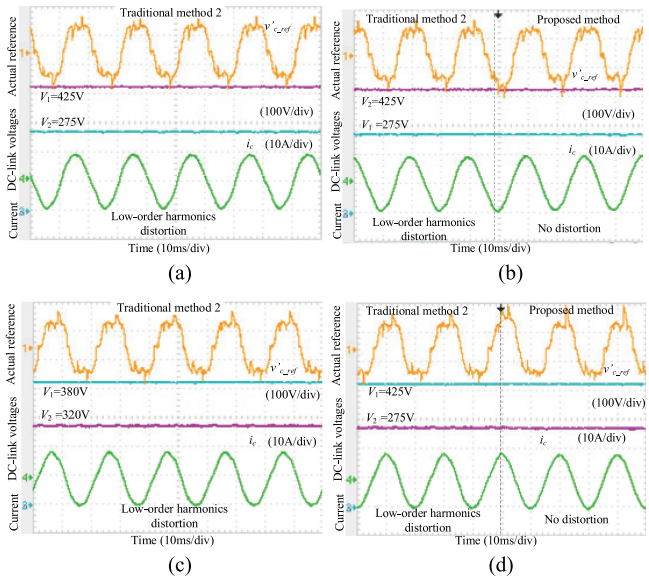

Fig. 20. Performance of the proposed method comparing with traditional method 2 when two dc-link voltages are unbalanced. (a) Using traditional method 2 in case one. (b) Comparison proposed method with traditional method 2 in case one. (c) Using traditional method 2 in case two. (d) Comparison proposed method with traditional method 2 in case two.

to maintain grid currents behavior as sinusoidal waveforms according to the unbalanced factor.

Fig. 20 shows the comparison of experiment results between traditional method 2 and proposed zero-sequence component injection method when two dc-link voltages are unbalanced. The current distortion around the zero-crossing point has been solved by compensation using traditional method 2. However, low-order harmonics distortions remain still, as shown

TABLE VI
THD COMPARISON OF THREE DIFFERENT METHODS

DC-link voltages	$V_1 = V_2$ = 350 V	V_1 = 380 V, V_2 = 320 V	V_1 = 425 V, V_2 = 275 V	V_1 = 320 V, V_2 = 380 V	V_1 = 275 V, V_2 = 425 V
Traditional method 1	4.3%	6.1%	12.0%	6.2%	11.6%
Traditional method 2	1.1%	5.3%	7.2%	5.4%	7.5%
Proposed method	1.1%	1.2%	1.4%	1.3%	1.4%

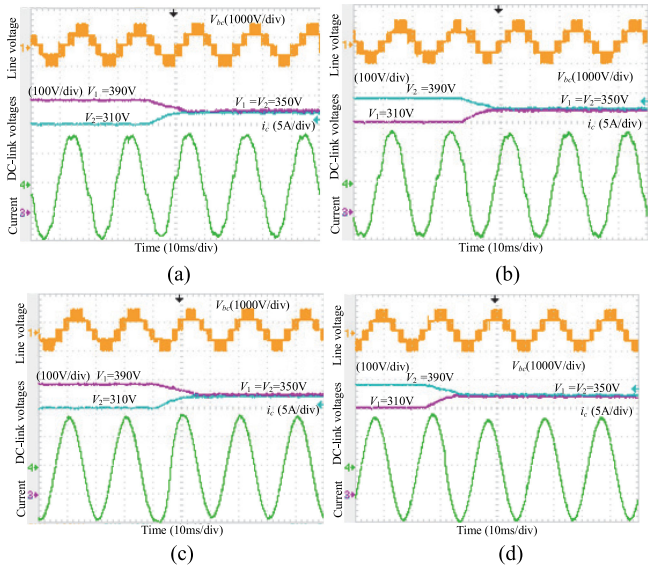

Fig. 21. Performance of the proposed method for the NP voltage balancing control. (a) ΔV is regulated at 0 V from 80 V using the traditional method. (b) ΔV is regulated at 0 V from –80 V using the traditional method. (c) ΔV is regulated at 0 V from 80 V using the proposed method. (d) ΔV is regulated at 0 V from –80 V using the proposed method.

in Fig. 20(a) and (c). Comparing with traditional method 2, the proposed method has the capability to mitigate the low-order harmonics of the input current for the Vienna rectifier when the imbalance occurs. Hence, the distortions in input currents are practically mitigated using the proposed method. Table VI shows the THD comparison of the assumed three methods.

To verify the performance for current harmonic mitigation in the transient state of dc-link voltages, the Vienna rectifier operates with the proposed zero-sequence component injection method. Transient response of unbalanced dc-link voltages for the Vienna rectifier as well as one-phase current and line-to-line voltage is presented in Fig. 21.

As shown in Fig. 21(a) and (b), it can be seen that the regulation of unbalanced dc-link voltages is realized by setting ΔV_{ref}. Comparing with balanced dc-link voltages, the waveform of the input current of the Vienna rectifier contains more serious distortion around the zero-crossing point caused by unbalanced factor and lagging angle using traditional method 1. Two dc-link voltages shown in Fig. 21(c) and (d) are controlled accurately and the same as that in Fig. 21(a) and (b). In the conclusion, the proposed method has no influence on

the control of the neutral-point voltage balance. Furthermore, there is no distortion in input current when dc-link voltages are balanced or unbalanced for steady-state and transient operation using the proposed zero-sequence component injection method.

V. Conclusion

This paper proposes a novel zero-sequence component injection method to mitigate the input current distortion of the Vienna rectifier with balanced or unbalanced dc-link voltages. A detailed model of the Vienna rectifier is presented to explain the generation mechanism of the current distortion. For industrial application, the proposed method simplifies the identification of the abnormal interval without complicated calculation in a slant and asymmetrical space vector diagram. Due to lagging angle and unbalanced factor, these abnormal intervals are decided once by comparing the average duties with 0 or 1. Besides, the average duties are modified by adding the compensations in the abnormal interval where current distortions occur. Based on the unbalanced factor, three compensation components for three-phase average duties are unequal to each other and first analyzed quantitatively. In the two-stage system including ac–dc stage and buck-type dc–dc stage, it is recommended to use 700 V or higher voltage level as the dc-link voltage, which has at least 30% margin of headroom to be able to add compensation components to improve the performance of the proposed method. Moreover, theoretical analysis and experimental verification demonstrate the performance of the proposed method. The current harmonics of the Vienna rectifier are mitigated significantly in steady and transient states of dc-link voltages. In addition, the proposed method has no effect on the control of the neutral-point voltage balance.

Appendix

This Appendix presents the derivation of inequality (18) and (19).

Based on the inequality (17), the maximal and minimal values of d_x ($x = a$, b, and c) are defined as $d_{x\_\max}$ and $d_{x\_\min}$, respectively. They can be expressed as

$$\begin{cases} d_{a\_\max} = \frac{\frac{\sqrt{3}}{2}m+k}{1+k} \\ d_{a\_\min} = \frac{\frac{3}{4}m+k}{1+k} \\ d_{b\_\max} = \frac{-\frac{3}{4}m+k}{1-k}+1 \\ d_{b\_\min} = \frac{-\frac{\sqrt{3}}{2}m+k}{1-k}+1 \\ d_{c\_\max} = \frac{\frac{3}{2}m\sin\varphi+k}{1-k}+1 \\ d_{c\_\min} = \frac{-\frac{3}{4}m+k}{1-k}+1 \end{cases}. \tag{A-1}$$

According to (A-1), the existing conditions of k and m to ensure all three-phase average duties (d_a, d_b, and d_c) in the range of [0, 1] are as follows:

$$\begin{cases} 0 \le d_a \le 1 \\ 0 \le d_b \le 1 \\ 0 \le d_c \le 1 \end{cases}. \tag{A-2}$$

Because k is in the range of (–1, 1), both $(1 + k)$ and $(1 – k)$ are larger than zero. Thus, the following equation is obtained easily for $d_{a\_\max} \le 1$ and $d_{b\_\min} \ge 0$:

$$\frac{\sqrt{3}}{2}m \le 1. \tag{A-3}$$

For $d_{c\_\max} \le 1$, the following equation should be satisfied as well:

$$-\frac{3}{4}m + 1 \ge 0. \tag{A-4}$$

Using zero-sequence component injection modulation, it is found that the inequalities (A-2)–(A-4) are always satisfied, because m is in the range of $[0, 2/\sqrt{3}]$. In the same way, the following equations should be satisfied for $d_{a\_\min} \ge 0$ and $d_{b\_\max} \le 1$, respectively:

$$k \ge -\frac{3}{4}m \tag{A-5}$$

$$k \le \frac{3}{4}m. \tag{A-6}$$

By incorporating (A-5) and (A-6), inequality (18) can be obtained. In specific, the inequality (19) can be easily attained for $d_{c\_\min} \ge 0$.

References

[1] H. Chen and D. C. Aliprantis, "Analysis of squirrel-cage induction generator with Vienna rectifier for wind energy conversion system," *IEEE Trans. Energy Convers.*, vol. 26, no. 3, pp. 967–975, Sep. 2011.

[2] W. Ding, B. Duan, Y. Li, J. Liu, and C. Zhang, "Design of three-phase PWM converter in the battery pack testing system using fractional-order control," in *Proc. IEEE 8th Int. Power Electron. Motion Control Conf.*, 2016, pp. 2582–2588.

[3] L. Dalessandro, S. D. Round, and J. W. Kolar, "Center-point voltage balancing of hysteresis current controlled three-level PWM rectifiers," *IEEE Trans. Power Electron.*, vol. 23, no. 5, pp. 2477–2488, Sep. 2008.

[4] J. W. Kolar and T. Friedli, "The essence of three-phase PFC rectifier systems—Part I," *IEEE Trans. Power Electron.*, vol. 28, no. 1, pp. 176–198, Jan. 2013.

[5] M. Hartmann, S. D. Round, H. Ertl, and J. W. Kolar, "Digital current controller for a 1 MHz, 10 kW three-phase Vienna rectifier," *IEEE Trans. Power Electron.*, vol. 24, no. 11, pp. 2496–2508, Nov. 2009.

[6] R. Burgos, R. Lai, Y. Pei, F. Wang, D. Boroyevich, and J. Pou, "Space vector modulation for Vienna-type rectifiers based on the equivalence between two- and three-level converters: a carrier-based implementation," *IEEE Trans. Power Electron.*, vol. 23, no. 4, pp. 1888–1898, Jul. 2008.

[7] L. Hang, B. Li, M. Zhang, Y. Wang, and L. M. Tolbert, "Equivalence of SVM and carrier-based PWM in three-phase/wire/level Vienna rectifier and capability of unbalanced-load control," *IEEE Trans. Ind. Electron.*, vol. 61, no. 1, pp. 20–28, Jan. 2014.

[8] J. W. Kolar and F. C. Zach, "A novel three-phase utility interface minimizing line current harmonics of high-power telecommunications rectifier modules," *IEEE Trans. Ind. Electron.*, vol. 44, no. 4, pp. 456–466, Aug. 1997.

[9] N. C. Foureaux, J. H. Oliveira, F. D. De Oliveira, B. De J. Cardoso Filho, and R. S. De Faria, "Command generation for wide range operation of hysteresis controlled Vienna rectifiers," *IEEE Trans. Ind. Appl.*, vol. 5, no. 3, pp. 2373–2380, May 2015.

[10] A. Rajaei, M. Mohamadian, and A. Y. Varjani, "Vienna-rectifier-based direct torque control of PMSG for wind energy application," *IEEE Trans. Ind. Electron.*, vol. 60, no. 7, pp. 2919–2929, Jul. 2013.

[11] L. Dalessandro, S. D. Round, U. Drofenik, and J. W. Kolar, "Discontinuous space-vector modulation for three-level PWM rectifiers," *IEEE Trans. Power Electron.*, vol. 23, no. 2, pp. 530–542, Mar. 2008.

[12] J. Lee and K. Lee, "A novel carrier-based PWM method for Vienna rectifier with a variable power factor," *IEEE Trans. Ind. Electron.*, vol. 63, no. 1, pp. 3–12, 2015.

[13] J. Lee and K. Lee, "Carrier-based discontinuous PWM method for Vienna rectifiers," *IEEE Trans. Power Electron.*, vol. 30, no. 6, pp. 2896–2900, Jun. 2015.
[14] J. Lee and K. Lee, "Performance analysis of carrier-based discontinuous PWM method for Vienna rectifiers with neutral-point voltage balance," *IEEE Trans. Power Electron.*, vol. 31, no. 6, pp. 4075–4084, Jun. 2016.
[15] N. Backman and R. Rojas, "Modern circuit topology enables compact power factor corrected three-phase rectifier module," in *Proc. 24th Int. Telecommun. Energy Conf.*, 2002, pp. 107–114.
[16] R. Lai, F. Wang, R. Burgos, D. Boroyevich, D. Jiang, and D. Zhang, "Average modeling and control design for VIENNA-type rectifiers considering the dc-link voltage balance," *IEEE Trans. Power Electron.*, vol. 24, no. 11, pp. 2509–2522, Nov. 2009.
[17] W. Song *et al.*, "A hybrid control method to suppress the three times fundamental frequency neutral-point voltage fluctuation in a Vienna rectifier," *IEEE J. Emerging Select. Topics Power Electron.*, vol. 4, no. 2, pp. 468–480, Jun. 2016.
[18] X. Li, Y. Sun, H. Wang, M. Su, and S. Huang, "A hybrid control scheme for three-phase Vienna rectifiers," *IEEE Trans. Power Electron.*, vol. 33, no. 1, pp. 629–640, Jan. 2018.
[19] J. Lee and K. Lee, "Predictive control of Vienna rectifiers for PMSG systems," *IEEE Trans. Ind. Electron.*, vol. 64, no. 4, pp. 2580–2591, Apr. 2017.
[20] H. Wu, J. Wang, T. Liu, and Y. Xing, "Modified SVPWM controlled three-port three-phase ac-dc converters with reduced power conversion stages for wide voltage range applications," *IEEE Trans. Power Electron.*, to be published, 2017, doi 10.1109/TPEL.2017.2761906.
[21] J. Adhikari, P. Iv, and S. K. Panda, "Reduction of input current harmonic distortions and balancing of output voltages of the Vienna rectifier under supply voltage disturbances," *IEEE Trans. Power Electron.*, vol. 32, no. 7, pp. 5802–5812, Jul. 2017.
[22] Y. Park, S. K. Sul, C. H. Lim, W. C. Kim, and S. H. Lee, "Asymmetric control of dc-link voltages for separate MPPTs in three-level inverters," *IEEE Trans. Power Electron.*, vol. 28, no. 6, pp. 2760–2769, Jun. 2013.
[23] U. Choi, F. Blaabjerg, and K. Lee, "Control strategy of two capacitor voltages for separate MPPTs in photovoltaic systems," *IEEE Trans. Ind. Appl.*, vol. 51, no. 4, pp. 3295–3303, Jul. 2015.
[24] Z. Zhang, A. Chen, X. Xing, and C. Zhang, "Space vector modulation based control strategy of three-level inverter for separate MPPTs in photovoltaic system," in *Proc. IEEE 8th Int. Power Electron. Motion Control Conf.*, 2016, pp. 2394–2400.
[25] W. Ding, J. Liu, H. Qiu, B. Duan, and C. Zhang, "Independent voltage outputs control for Vienna rectifier considering multiple loads situations," in *Proc. IEEE 3rd Int. Future Energy Electron. Conf., ECCE Asia*, 2017, pp. 1785–1790.
[26] W. L. Ming and Q. C. Zhong, "A single-phase rectifier having two independent voltage outputs with reduced fundamental frequency voltage ripples," *IEEE Trans. Power Electron.*, vol. 30, no. 7, pp. 3662–3673, Jul. 2015.
[27] Z. Ye, Y. Xu, X. Wu, G. Tan, X. Deng, and Z. Wang, "A simplified PWM strategy for a neutral-point-clamped (NPC) three-level converter with unbalanced dc links," *IEEE Trans. Power Electron.*, vol. 31, no. 4, pp. 3227–3238, Apr. 2016.
[28] X. Wu, G. Tan, Z. Ye, G. Yao, Z. Liu, and G. Liu, "A virtual-space-vector PWM for three-level neutral-point-clamped inverter with unbalanced dc-links," *IEEE Trans. Power Electron.*, vol. 33, no. 3, pp. 2630–2642, Mar. 2018.

Wenlong Ding (S'17) was born in Linyi, China, in 1988. He received the B.S. and M.S. degrees in control theory and control engineering from Qufu Normal University, Jining, China, in 2011 and 2014, respectively. He is currently working toward the Ph.D. degree in electrical engineering at the School of Control Science and Engineering, Shandong University, Jinan, China.

His current research interests include multilevel converters, power conversion, and battery charging technology.

Chenghui Zhang (M'14–SM'18) received the Bachelor's and Master's degrees in automation engineering from the Shandong University of Technology, Jinan, China, and the Ph.D. degree in control theory and operational research from Shandong University, Jinan, in 1985, 1988, and 2001, respectively.

In 1988, he joined Shandong University, where he is currently a Professor in the School of Control Science and Engineering, the Chief Manager of Power Electronic Energy-Saving Technology and Equipment Research Center of Education Ministry, a Specially Invited Cheung Kong Scholars Professor by China Ministry of Education, and a Taishan Scholar Special Adjunct Professor. He is also one of the state-level candidates of "The New Century National Hundred, Thousand and Ten Thousand Talent Project," the Academic Leader of Innovation Team of Ministry of Education, and the Chief Expert of the National "863" high technological planning. His research interests include optimal control of engineering, power electronics and motor drives, energy-saving techniques, and time-delay systems.

Feng Gao (S'07–M'09) received the B.Eng. and M.Eng. degrees from Shandong University, Jinan, China, in 2002 and 2005, respectively, and the Ph.D. degree from the School of Electrical and Electronic Engineering, Nanyang Technological University, Singapore, in 2009, all in electrical engineering.

From September 2006 to February 2007, he was a Visiting Scholar with the Institute of Energy Technology, Aalborg University, Aalborg, Denmark. From 2008 to 2009, he was a Research Fellow with Nanyang Technological University. Since 2010, he has been with the School of Electrical Engineering, Shandong University, where he is currently a Professor and the Vice Dean.

Dr. Gao was a recipient of the IEEE Industry Applications Society Industrial Power Converter Committee Prize for a paper published in 2006, and he is currently serving as an Associate Editor for the IEEE TRANSACTIONS ON POWER ELECTRONICS.

Bin Duan (M'18) received the B.S. degree in automation and the Ph.D. degree in control theory and control engineering from Shandong University, Jinan, China, in 2005 and 2010, respectively.

In 2010, he joined Shandong University, where he is currently an Associate Professor with the School of Control Science and Engineering. His current research interests include power electronics, battery technology, modeling, and optimal control of complex nonlinear systems.

Han Qiu was born in Yantai, China, in 1993. He received the B.S. degree in automation from the School of Control Science and Engineering, Shandong University, Jinan, China, in 2016. He is currently working toward the M.S. degree in power electronics.

His current research interests include Vienna rectifier and bipolar dc–dc converters.